Programming emissivity on fully integrated VO_2 windows

José Figueroa[1], Yunqi Cao[1], Tongyu Wang[1], David Torres[1] and Nelson Sepúlveda[1*]

Department of Electrical and Computer Engineering, Michigan State University, East Lansing, Michigan, 48824

DOI: 10.5185/amlett.2018.1848
www.vbripress.com/aml

Abstract

The programmability of emissivity states in a monolithically integrated micro window based on vanadium dioxide (VO_2) thin film is demonstrated. The 400 μm window features a VO_2 thin film with integrated electrodes for actuation and sensing. The phase transition was induced by resistive heating, while the electrical resistivity and optical transmittance (for near IR wavelength of 1550 nm) of the VO_2 thin film were monitored simultaneously. Abrupt drops in electrical resistance and optical transmittance confirmed the quality of the VO_2 thin film. Electronic pulses were used to program emissivity states in the VO_2 window. The emissivity programmed state was shown for a specific DC current over imposed with the programming pulse; but any emissivity state that belongs to the minor hysteretic curves can be obtained by choosing different electronic inputs. The fully monolithically integrated device presented here can be used for IR cloaking applications, where different emissivity values can be programmed with electronic pulses. Copyright © 2018 VBRI Press.

Keywords: Emissivity, smart materials, vanadium dioxide.

Introduction

In the last few years, adaptive camouflage has seen an increase interest for its wide array of applications. Many animals have natural camouflage capabilities for survival and hunting. Species such as cephalopods and reptiles, use a form of visual coloration to adapt to any surroundings [1–3]. Numerous past studies have tried to discern and incorporate such adaptive camouflage for commercial and military grade applications [4]. Similarly, infrared cloaking is of equal importance due to the ability to cloak and shape shift in thermal imaging which allows to incorporate any camouflage system on arbitrary surfaces [5–7]. In order to create a thermal cloaking device, either the temperature or the emissivity of the material must be modulated [8,9]. Emissivity modulation is more advantageous over thermal controlling, since it would not involve a real temperature change of the object and it will eliminate the need to compensate for heat dissipation limitations when controlling the temperature. However, emissivity modulation would require materials with tunable optical properties, especially for the thermal infra-red (IR) region.

Vanadium dioxide (VO_2), has shown to be a suitable candidate for such applications. It undergoes an insulator to metal phase transition above 68 ℃ [10], which can be done either by simple conductive, resistive heating, or photo-thermal heating [11–13]. Along with the phase transition, VO_2's optical and electrical properties simultaneously change as well [14-15]. The material's optical constants (n, k) suffer a significant change across the phase transition, abruptly causing a drop in transmittance. This change is more evident for near-IR (NIR) region up to 2500 nm [16,17], thus allowing VO_2 to be incorporated in smart window designs [18–21]. This was cleverly used by Xiao et al., when they reported the use of VO_2 for thermally adaptive camouflage. [8]. VO_2 also behaves as a highly disordered material for emissivity modulation, due to its change in emittance along the phase transition [22,23]. Furthermore, unlike most materials, VO_2's emissivity decreases as the temperature increases through the phase transition region. This means that the material "looks colder" as the temperature is raised. Since the transition region of VO_2 extends only about 10 °C, inducing the change in emissivity of a VO_2 thin film coating requires much less energy than changing the emissivity of the coated element by a large increase in temperature. This makes VO_2 a great candidate for adaptive camouflage windows.

Here we propose a micro variable optical window based on VO_2 thin film. The window can be actuated via resistive heating which allows to program states in both transmittance and emissivity via electronic modulation. Via this change in transmittance and emissivity we can developed a smart VO_2 window that could act as a cloaking device. The intrinsic hysteresis of VO_2 allows for multiple optical states for a single temperature within the transition region. In this work, we exploit this to demonstrate electronically programmable emissivity states in a monolithically integrated VO_2 window.

Experimental

Device Fabrication

The fabrication of the VO_2-based window consisted of a 4-mask lithography process, with a minimum feature size of 10 μm. The fabrication process is shown in **Fig. 1.** A double sided polished SiO_2 wafer (2-inch diameter, 500 μm thick, SOF50D05C2, MTI) was used as the substrate. The metal layers (titanium/platinum (Ti/Pt) with thicknesses of $400\,Å/1500Å$, respectively) used for the heater and electrodes were deposited by evaporation and patterned using lift-off technique. The Ti layer was used only for adhesion purposes. The width of the heater loop was 10 μm and the electrodes was 15 μm. The gap between the heater loop and the electrode was 10 μm as well.

An insulating layer of SiO_2 of approximately 400 nm thick was deposited by plasma enhanced chemical deposition (PECVD). This was done in 3 steps of ~ 130 nm each to avoid possible voids through the SiO_2. After deposition, the SiO_2 layer was etched by reactive ion etching (RIE) to open vias to the Pt electrodes to the VO_2 thin film that was going to be deposited next. A layer of VO_2, approximately 170 nm thick was deposited by pulsed laser deposition (PLD). A KrF laser operated at 10 Hz with a laser fluence of ~2 J/cm^2 was used, with a deposition time of 25 minutes. The substrate was maintained at 595 ℃ in an oxygen environment at 15 mTorr pressure. After deposition, an annealing process under the same pressure and temperature conditions was performed for 30 minutes. To avoid any undesired material residual accumulation that would have affected the results for transmission experiments, the backside of the wafer was covered during the deposition. This was followed by the patterning of the VO_2 windows through photolithography process and RIE using [24]. Finally, another SiO_2 etching step was performed to open contact pads to the heater and electrodes. The 2 inch wafer was then diced into individual dies, each measuring 4 mm^2.

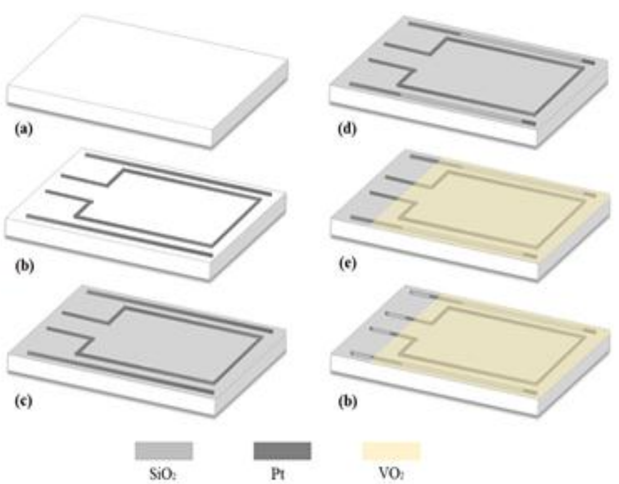

Fig. (1). Fabrication process for the VO_2 based window. (a) SiO_2 substrate, (b) metallization of heater and electrodes. (c) SiO_2 insulating layer, (d) opening of the electrodes. (e) VO_2 deposition and window patterning, and (f) opening of contact pads for electrical connections.

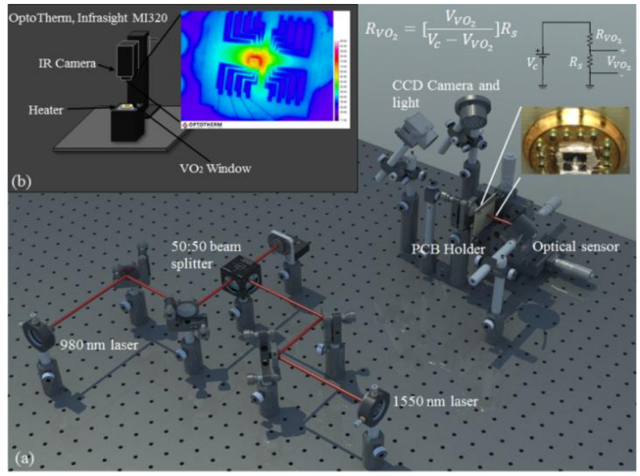

Fig. (2). Optical set-ups used to measure the VO_2 window: (a) Electro-optical setup used for measurement taking. (b) IR camera setup.

Experimental setup

Fig. 2 (a) shows the electro-optical setup used to test the VO_2 window. The die containing the four micro VO_2 windows was mounted and wire-bonded into a circular package which has a hole in the middle to facilitate the transmittance measurements. The package was then mounted to a custom built printed circuit board (PCB) with a centered hole and electrical connections for both the heater and electrodes. Once wired and mounted, the PCB was placed on an X-Y-Z translational stage to align the IR laser beam with incidence normal to the window. A Thorlabs NIR laser diode ($\lambda = 1550$ nm, ML925B45F) was operated below its stable power of 5 mW for measurement taking. To make sure that the beam spot was properly aligned with the window, a Thorlabs NIR laser diode ($\lambda = 980$ nm, L980P010) was used. Both laser diodes were passed through a 50:50 NIR beam splitter (Thorlabs, BS015- 50:50, $1100\,\text{nm} - 1600\text{nm}$), then coupled into a single mode optical fiber and focused with a lens of 15 mm focal length. The lens was mounted on a micro positioner rail to control the diameter of the beam. A laser beam profiler (LBP, Newport, Model number LBP-4-PCI) was used to assist in the alignment of the focused laser beam and to obtain an approximate value of the beam diameter. After passing through the sample, the laser beam was focused into an optical sensor (S144C, Thorlabs) connected to a power meter (PM100D, Thorlabs), which communicates with a LabVIEW computer interface to facilitate data gathering.

For measurements, the electrical contacts on the PCB were connected to a National Instruments data acquisition (NI USB-6001) control for data acquisition. To actuate the window, a heater current I_H was used while the voltage across the VO_2 (V_{VO_2}) was measured. Using a voltage divider and V_{VO_2}, the resistance of VO_2 was calculated (see insert in **Fig. 2**). For the voltage divider, a series resistor of $R_S = 6.67\,k\Omega$ and a supply voltage of $V_C = 10\,V$ were used to measure the VO_2 resistance. Thus, the setup allows to simultaneously measure and drive the device.

The electro-thermal actuation, temperature distribution and emissivity were investigated by IR thermal imaging (OptoTherm, Infrasight MI320) as shown in **Fig. 2 (b)**. Emissivity measurements were taken as a function of both temperature (i.e. conductive heating) and current (i.e. resistive, or Joule heating). For the temperature measurements, the die containing the window was attached to a Peltier heater. In order to obtain the value of the thermal emissivity, it is necessary to have a material with a well-defined emissivity (i.e. a benchmark). To this end, a piece of masking tape with a known value of emissivity ($\mathrm{E} = 0.95$ [25]) was placed near the window of VO_2. Then the emissivity of the VO_2 was modified in the thermal camera until the temperature measured by the IR thermal imaging system in the VO_2 region was equal to the temperature measured in a selected region inside the masking tape.

Results and discussion

Characterization of both optical and electrical transitions were performed simultaneously for the 400 μm sized VO_2 window as shown in **Fig. 3**. In order to obtain the major hysteretic loops, current steps of increasing amplitude (0.1 V, or 0.63 mA) were applied to the heater electrodes until the phase transition was complete. This resulted in the major heating hysteretic loop. Then, current steps of decreasing amplitude were applied until reaching 0 mA, which resulted in the major cooling hysteretic loop. Each current step lasted 1 s, and the measurement was taken after waiting 900 ms from the beginning of the step. During this input to the heater, the VO_2's resistance and transmittance were being monitored. A drop of approximately 3 orders in magnitude is visible for the resistance of VO_2 across its phase transition. This drop in resistance of VO_2 is to be expected and confirms the overall good quality of the sample. The average resistance drop for the sample was from $R_i = 631\ k\Omega$ to $R_f = 676\ \Omega$, having an average $\frac{R_i}{R_f}$ ratio of ~ 935 . For the optical transmittance, the power of the IR laser before the sample (1.22 mW) was used to normalize the transmitted power through the sample. A transmittance drop from $T_i = 0.36$ to $T_f = 0.14$ was observed for the 400 μm window, giving a ratio of $\frac{T_i}{T_f} = 2.57$ for the infrared region ($\lambda = 1550\ nm$). To demonstrate the programmability stages of VO_2, several minor loops were measured for both electrical and optical transitions. **Fig. 4** shows the plots for resistance and transmittance. The input used for obtaining these minor loops is shown in the insert of **Fig. 4**.

Obtaining the minor loop plots allows for a more reliable way to program the desired values for transmittance and therefore emissivity. For this case, the same current-increase input steps used to obtain the major heating hysteretic loop was used, until reaching 15 mA.

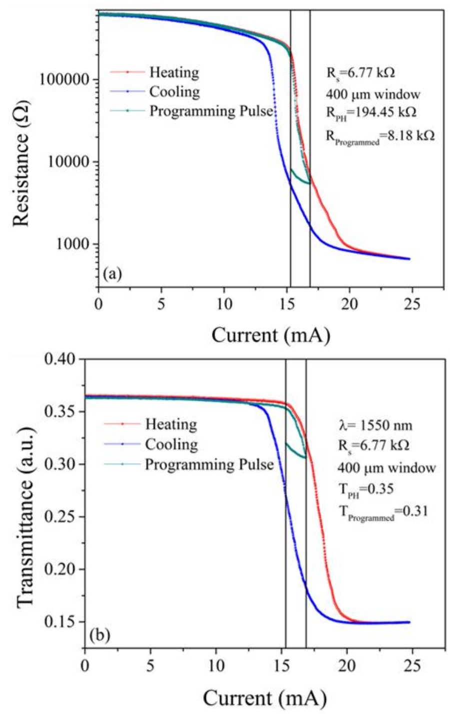

Fig. (3). Simultaneous measurements for the electrical (a) and optical (b) transition in the 400 μm VO_2 window.

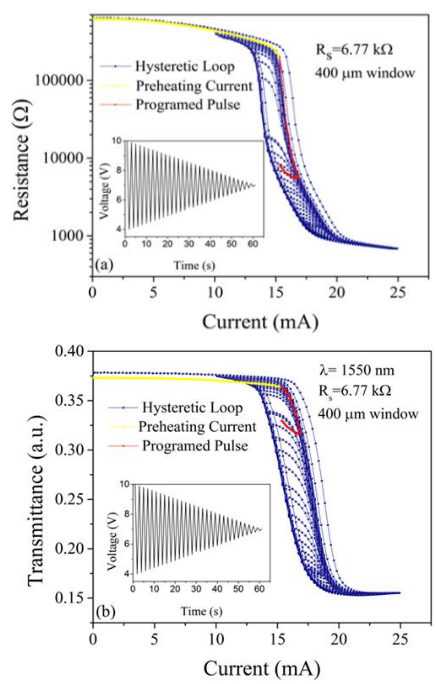

Fig. 4. Electrical (a) and optical transition (b) minor loops in the 400 μm VO_2 window. Programming pulse is over-imposed. Inset shows the voltage input used to obtain the minor loops.

This was used as the pre-heating current, from which the first electrical/optical state was measured. Programming of a second electrical/optical state was achieved by applying an electrical pulse (also following the same step input) up to 16.97 mA **(see Fig. 3).** Since this value of current is not enough to complete the phase transition of VO_2, once the pulse is over, the resistance and transmittance comes back to the pre-heating current, but following one of the minor hysteretic loops. The resulting pre-heated and programmed states in electrical resistance and optical transmittance are shown in **Fig. 3,** and the corresponding minor loop is identified in **Fig. 4.** It should be noted that there is a DC shift in transmittance between the minor loops and the programming pulse, which is most likely due to a small difference in the background light when measurements were taken. Although this shows only one programmed state, essentially any electrical resistance/transmittance value that belongs to the minor loops can be programmed by simply using a different pulse magnitude or pre-heating current.

In order to know the required minimum sampling rate for the $400\,\mu m$ window, the device's thermal time constant was measured. This was done by measuring the voltage in VO_2 (V_{VO2}) resulting from a single current step input I_H. **Fig. (5)** shows the thermal time constant ($\tau_{off} = 21.68\,ms$) for the device for the case when the step was released **(see Fig. 5).** This measured time constant of ~ 20 ms is much faster than the 100 ms used for the current step input pulses, which indicates that the pulses will be enough to reach steady-state.

The change in VO_2's optical properties across its phase transition is larger for wavelengths in the infra-red (IR) region [18]. The material's ability to radiate thermal energy (i.e. emissivity) also changes abruptly during the material's phase change, which allows for selective thermal emission. **Fig. 6 shows** the VO_2 emissivity as a function of both temperature and current. For both plots, VO_2 shows negative differential emissivity at the onset of the phase transition, which occurs around $T_{PT} \approx 68\,℃$ and $I_{PT} \approx 19.9\,mA$. The VO_2 window shows a large thermal emissivity change from 0.76 below the transition point to 0.54 above the transition point. To measure emissivity as a function of current, the temperature of the VO_2 window was first measured as a function of current. Given that the emissivity of VO_2 changes with temperature, we needed a benchmark for calibration. Using the masking tape mentioned earlier for conductive experiments from Peltier heater would not work in this case, since it would require increasing the temperature of the tape by Joule heating through the same resistive heater used for the window. Therefore, we used the platinum heater as a temperature sensor, by monitoring its resistance as the current was applied. The heater's temperature as a function of current was used to obtain the VO_2 window's temperature. This allowed for mapping VO_2's emissivity to obtain figure (6-b). On comparing the transition point for the plots on Fig. (4) to the plot in Fig. (6-b), there is a difference in current of $I_{PT} \approx 4.5\,mA$. This is most likely due to the method for measuring the emissivity as a function of current as previously mentioned. It should be noted that the hysteresis curves have similar shapes, which suggests that the difference is most likely a "DC offset", which would be corrected by an additional integrated device that can be used as a benchmark for calibration.

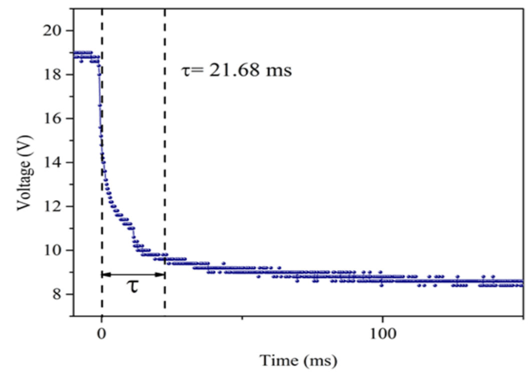

Fig. 5. Time constant measurement for the 400 μm window.

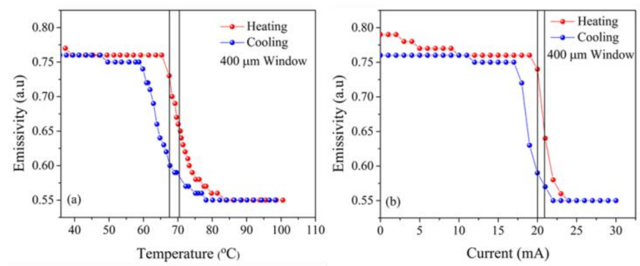

Fig. 6. Emissivity as a function of temperature (a) and current (b) for the 400 μm window.

Fig. (7) shows a thermal image for a $400\,\mu m$ window before and after actuation using an electric pulse (1 mA), supplied in the form of short current steps –as depicted for the electrical and transmissivity experiments. Although both states correspond to the same temperature –since after the pulse the current returns to the pre-heated value–, the thermal image after the pulse clearly shows a lower irradiance, which is mapped to a lower temperature. This is due to the lower emissivity of the VO_2 after the programming pulse.

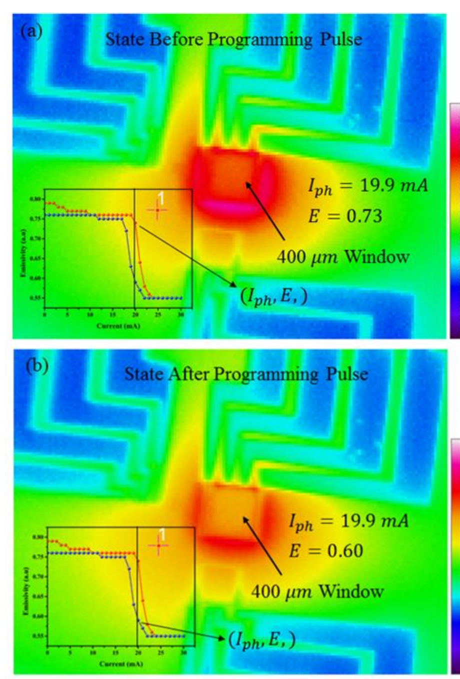

Fig. 7. Thermal image for the 400 μm window before programming pulse (a), and after programming pulse (b).

Conclusion

We have developed a VO_2 based window of 400 μm^2 that can be used as a smart window or thermal camouflage system. The electrical and optical transition in VO_2 where investigated, and hysteretic curves for minor loops where obtained. The minor loops inside the hysteresis of the VO_2 allows to program any state for transmissivity inside the window. Since the optical properties of VO_2 change greatly in the IR- region, then the emissivity will change during the transition. The emissivity for the VO_2 film as a function of both temperature and current was determined, and confirmed that the film shows a negative differential emissivity with the phase change. Emissivity states were programmed by electronic pulses to change the window's thermal radiation, which can be used for real-time thermal cloaking. The rapid tune-ability of both transmissivity and emissivity in VO_2 suggest that the film could be incorporated in the use of adaptive thermal camouflage devices.

Acknowledgements

This work was supported in part by the National Science Foundation (USA), Award Number: 1744273. The authors are thankful to N. Davila and E. Merced for assistance in the VO2 window design.

Author's contributions

Conceived the plan: J.F., Y.C., and N.S.; Performed the expeirments: J. F. and Y. C.; Data analysis: J. F. and T. W., and D.T.; Wrote the paper: J.F., Y.C, T.W, D.T., and N.S. Authors have no competing financial interests.

References

1. D. M. Stuart-Fox and A. Moussalli, *Animal Camouflage Mechanisms and Function* (2011).
2. B. W. Jones and M. K. Nishiguchi, Mar. Biol. 144, 1151 (2004).
3. H. Nilsson Sköld, S. Aspengren, and M. Wallin, Pigment Cell Melanoma Res. 26, 29 (2013).
4. C. Yu, Y. Li, X. Zhang, X. Huang, V. Malyarchuk, S. Wang, Y. Shi, L. Gao, Y. Su, Y. Zhang, H. Xu, R. T. Hanlon, Y. Huang, and J. A. Rogers, Proc. Natl. Acad. Sci. 111, 12998 (2014).
5. L. Phan, W. G. Walkup IV, D. D. Ordinario, E. Karshalev, J. M. Jocson, A. M. Burke, and A. A. Gorodetsky, Adv. Mater. 25, 5621 (2013).
6. K. K. Gupta, A. Nishkam, and N. Kasturiya, J. Ind. Text. 31, 27 (2001).
7. U. Leonhardt, Nature 498, 440 (2013).
8. L. Xiao, H. Ma, J. Liu, W. Zhao, Y. Jia, Q. Zhao, K. Liu, Y. Wu, Y. Wei, S. Fan, and K. Jiang, Nano Lett. 15, 8365 (2015).
9. T. Han, X. Bai, J. T. L. Thong, B. Li, and C. W. Qiu, Adv. Mater. 26, 1731 (2014).
10. F. J. Morin, Phys. Rev. Lett. 3, 34 (1959).
11. R. Cabrera, E. Merced, and N. Sepúlveda, J. Microelectromechanical Syst. 23, 243 (2014).
12. E. Merced, D. Noraica, D. Torres, R. Cabrera, F. E. Fernandez, and N. Sepulveda, Smart Mater. Struct. 105009, (2012).
13. S. Lysenko, a. Rúa, V. Vikhnin, F. Fernández, and H. Liu, Phys. Rev. B 76, 1 (2007).
14. Z. Tao, T.-R. Han, S. Mahanti, P. Duxbury, F. Yuan, C.-Y. Ruan, K. Wang, and J. Wu, Phys. Rev. Lett. 109, 1 (2012).
15. S. Lysenko, V. Vikhnin, F. Fernandez, a. Rua, and H. Liu, Phys. Rev. B - Condens. Matter Mater. Phys. 75, 1 (2007).
16. A. S. Barker, H. W. Verleur, and H. J. Guggenheim, Phys. Rev. Lett. 36, 2137 (1976).
17. H. W. Verleur, A. S. Barker, and C. N. Berglund, Rev. Mod. Phys. 40, 737 (1968).
18. H. Kakiuchida, P. Jin, S. Nakao, and M. Tazawa, Jpn. J. Appl. Phys. 46, 3 (2007).
19. H. Kim, Y. Kim, K. S. Kim, H. Y. Jeong, A. Jang, S. H. Han, and K. I. M. E. T. Al, 5769 (2013).
20. J. Zhou, Y. Gao, Z. Zhang, H. Luo, C. Cao, Z. Chen, L. Dai, and X. Liu, Scientific Reports, 24, 1 (2013).
21. M. Benkahoul, M. Chaker, J. Margot, E. Haddad, R. Kruzelecky, B. Wong, W. Jamroz, and P. Poinas, Sol. Energy Mater. Sol. Cells 95, 3504 (2011).
22. M. A. Kats, R. Blanchard, S. Zhang, P. Genevet, C. Ko, S. Ramanathan, and F. Capasso, Phys. Rev. X 3, 1 (2014).
23. Z. Zhang, Y. Gao, H. Luo, L. Kang, Z. Chen, J. Du, M. Kanehira, Y. Zhang, and Z. L. Wang, Energy Environ. Sci. 4, 4290 (2011).
24. D. Torres, T. Wang, J. Zhang, X. Zhang, S. Dooley, X. Tan, H. Xie, and N. Sepulveda, J. Microelectromechanical Syst. 25, 780 (2016).
25. Optotherm, Inc. (2017, July 17). *Calculating Emissivity*. Retreived from http://www.optotherm.com/emiss-calculating.htm

